of nonradiative recombination paths and a change in the spin-injection probability. Acquiring this polarized photon intensity map of the surface required a current source with a large degree of polarization, a sample temperature of 100 K, and good collection optics to obtain a large enough photon signal to sample in tandem with the STM topography. With the use of the calculational method discussed earlier, the optical polarization measured at the step edge can be used to find the initial electron polarization. The electron polarization at the time of recombination is found to be ~8% (Fig. 4, upper half). From Eq. 1, the initial electron polarization is calculated to be ~16%. This corresponds to an IE of only 16% (Fig. 4, lower half). The dramatic decrease (by a factor of 6) in injection efficiency indicates that the step edge causes a substantial amount of spin-flip scattering. If we assume that the initial polarization state over the step is 100%, then we can calculate a local spin-relaxation lifetime by solving Eq. 1 for τ_s and relabeling it as τ_s^{step}

$$\tau_s^{step} = \tau\left[\frac{\rho_e(0)}{\rho_e(\tau)} - 1\right] \qquad (2)$$

After substitution, $\tau_s^{step} \approx \tau/12$, and in terms of the bulk spin-relaxation lifetime, $\tau_s^{step} \approx \tau_s/12$. This means that the step scatters spins 12 times faster than the bulk processes.

Little is known about why a particular defect, such as a step edge, disrupts the spin injection process. Previous findings show that midgap states decrease the carrier lifetime (*26*), which suggests that midgap states may play an important role in decreasing the spin-relaxation lifetime (*27*). In our situation, we have the ability to compare the spin-injection properties of the GaAs(110) terrace with a $[\bar{1}11]$-oriented step. The electronic properties of these two features are very different in an important and revealing way. First, the GaAs(110) terrace has no midgap states, making it appear electronically similar to bulk GaAs, so one might expect to obtain the bulk spin relaxation lifetime when injecting over a flat GaAs(110) terrace (*28*). Second, the $[\bar{1}11]$-oriented step is most likely a GaAs(111) surface, which does have midgap states; in fact, it is found to be metallic (*29*). This metallic property has two profound implications for understanding our results. Firstly, this indicates that there would be nonradiative, phonon channels to the valence band states, explaining the large decrease in light intensity. Secondly, the half-filled bonds would create unpaired spins which could substantially affect the spin-injection process through spin-spin scattering events, explaining the reduction in the spin-relaxation lifetime when injecting over the step. From this analysis the height of the step does play an important role, because higher steps would have a larger number of metallic-like bonds than shorter steps, thereby increasing the likelihood of spin- flip scattering events (*30*).

References and Notes

1. S. Datta, B. Das, *Appl. Phys. Lett.* **56**, 665 (1990).
2. G. A. Prinz, *Phys. Today* **48** (no. 4), 58 (1995).
3. D. D. Awschalom, J. M. Kikkawa, *Phys. Today* **52** (no. 6), 33 (1999).
4. H. Ohno, *Science* **281**, 951 (1998).
5. H. Ohno *et al.*, *Appl. Phys. Lett.* **69**, 363 (1996).
6. J. M. Kikkawa, D. D. Awschalom, *Nature* **397**, 139 (1999).
7. P. R. Hammar, B. R. Bennett, M. J. Yang, M. Johnson, *Phys. Rev. Lett.* **83**, 203 (1999).
8. S. Gardelis, C. G. Smith, C. H. W. Barnes, E. H. Linfield, D. A. Ritchie, *Phys. Rev. B* **60**, 7764 (1999).
9. R. Fiederling *et al.*, *Nature* **402**, 787 (1999).
10. Y. Ohno *et al.*, *Nature* **402**, 790 (1999).
11. B. T. Jonker *et al.*, *Phys. Rev. B* **62**, 8180 (2000).
12. R. Wiesendanger, *Scanning Probe Microscopy and Spectroscopy, Methods and Applications* (Cambridge Univ. Press, Cambridge, 1994).
13. R. Berndt *et al.*, *Phys. Rev. Lett.* **74**, 102 (1995).
14. P. Renaud, S. F. Alvarado, *Phys. Rev. B* **44**, 6340 (1991).
15. S. F. Alvarado, P. Renaud, *Phys. Rev. Lett.* **68**, 1387 (1992).
16. S. F. Alvarado, *Phys. Rev. Lett.* **75**, 513 (1995).
17. E. Kisker, W. Gudat, E. Kuhlmann, R. Clauberg, M. Campagna, *Phys. Rev. Lett.* **45**, 2053 (1980).
18. The tips were electrochemically etched under high magnification (×500) with a 10% HCl solution and then loaded into a UHV chamber (4×10^{-11} to 8×10^{-11} torr) that contains a commercially available variable-temperature STM. To remove any native oxide, the tips were then cleaned in situ with electron-beam heating and placed on the STM imaging stage, with the magnetization directed either away from or toward the surface of the sample. For control purposes, nonmagnetic single-crystal <111>-oriented W tips were also used. These were etched with NaOH but were otherwise prepared in the same manner as the Ni tips. The GaAs(110) surfaces were prepared by cleaving p-type GaAs(001) wafers [Zn doped, hole density (p) = 1.25×10^{19} cm^{-3}, carrier mobility (μ) = 100 cm^2/volt seconds (Vs), x-ray (004) linewidth <10 arc sec, and etch pit density <3000/cm^2 over 100% of the area] in situ, which produces a clean, nearly atomically flat cross-sectional (110) surface. The samples were then placed on the STM stage and cooled with a cold finger immersed in liquid nitrogen. The temperature of the STM stage was measured to be 77 K, and we estimate the sample temperature to be ≈ 100 K, whereas the STM tip is not cooled and is assumed to be at room temperature.
19. S. F. Alvarado, H. Riechert, N. E. Christensen, *Phys. Rev. Lett.* **55**, 2716 (1985).
20. B. Fromme, G. Baum, D. Gockel, W. Raith, *Phys. Rev. B* **40**, 12312 (1989).
21. G. E. Pikus, A. N. Titkov, in *Optical Orientation*, F. Meier, B. P. Zakharchenya, Eds. (Elsevier, New York, 1984), pp. 73–131.
22. D. T. Pierce, F. Meier, *Phys. Rev. B* **13**, 5484 (1976).
23. R. C. Miller, D. A. Kleinman, W. A. Nordland Jr., R. A. Logan, *Phys. Rev. B* **23**, 4399 (1981).
24. K. Zerrouati *et al.*, *Phys. Rev. B* **37**, 1334 (1988).
25. G. Schmidt, D. Ferrand, L. W. Molenkamp, A. T. Filip, B. J. van Wees, *Phys. Rev. B* **62**, R4790 (2000).
26. B. T. Jonker, O. J. Glembocki, R. T. Holm, R. J. Wagner, *Phys. Rev. Lett.* **79**, 4886 (1997).
27. M. W. J. Prins *et al.*, *J. Phys. Condens. Matter* **7**, 9447 (1995).
28. R. M. Feenstra, J. A. Stroscio, J. Tersoff, A. P. Fein, *Phys. Rev. Lett.* **58**, 1192 (1987).
29. D. K. Biegelsen, R. D. Bringans, J. E. Northrup, L. E. Swartz, *Phys. Rev. Lett.* **65**, 452 (1990).
30. We thank M. Klotz and S. Singh for their helpful comments. Supported by the Office of Naval Research (grant N00014-97-1-1058), NSF (grants DMR-9733994, DMR-0080054, and DMR-0102755), and Research Corporation (grant RI0153).

30 January 2001; accepted 11 April 2001

MgB$_2$ Superconducting Thin Films with a Transition Temperature of 39 Kelvin

W. N. Kang,* Hyeong-Jin Kim, Eun-Mi Choi, C. U. Jung, Sung-Ik Lee

We fabricated high-quality *c* axis–oriented epitaxial MgB$_2$ thin films using a pulsed laser deposition technique. The thin films grown on $(1\ \bar{1}\ 0\ 2)$ Al$_2$O$_3$ substrates have a transition temperature of 39 kelvin. The critical current density in zero field is ~6×10^6 amperes per cubic centimeter at 5 kelvin and ~3×10^5 amperes per cubic centimeter at 35 kelvin, which suggests that this compound has potential for electronic device applications, such as microwave devices and superconducting quantum interference devices. For the films deposited on Al$_2$O$_3$, x-ray diffraction patterns indicate a highly *c* axis–oriented crystal structure perpendicular to the substrate surface.

The recent discovery of the binary metallic MgB$_2$ superconductor (*1*) having a remarkably high transition temperature (T_c) of 39 K has attracted great scientific interest (*2–8*). With its metallic charge carrier density (*2*) and the strongly linked nature of its intergrains in a polycrystalline form (*9*, *10*), this material is a promising candidate for superconducting devices (*11*) as well as large-scale applications. Furthermore, because single-crystal growth of MgB$_2$ seems very difficult, the fabrication of epitaxial thin films should be an important development for future basic research studies.

National Creative Research Initiative Center for Superconductivity, Department of Physics, Pohang University of Science and Technology, Pohang 790–784, Korea.

*To whom correspondence should be addressed. E-mail: wnkang@postech.ac.kr

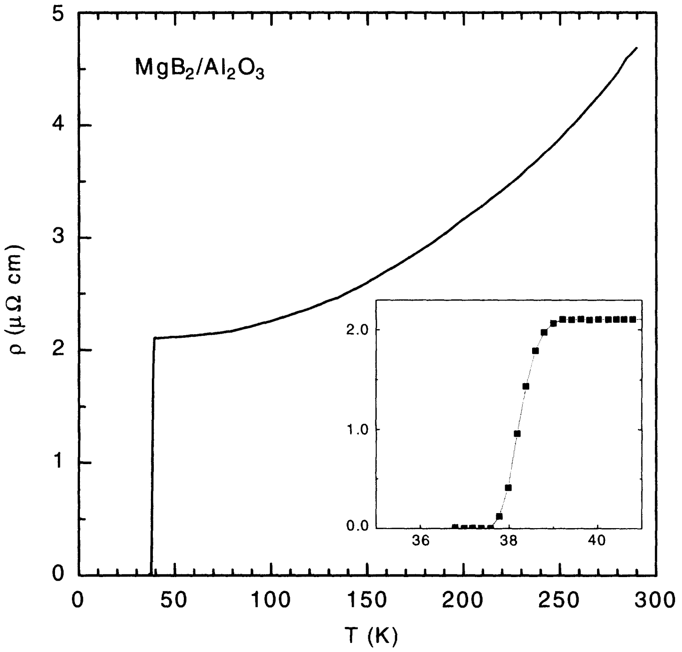

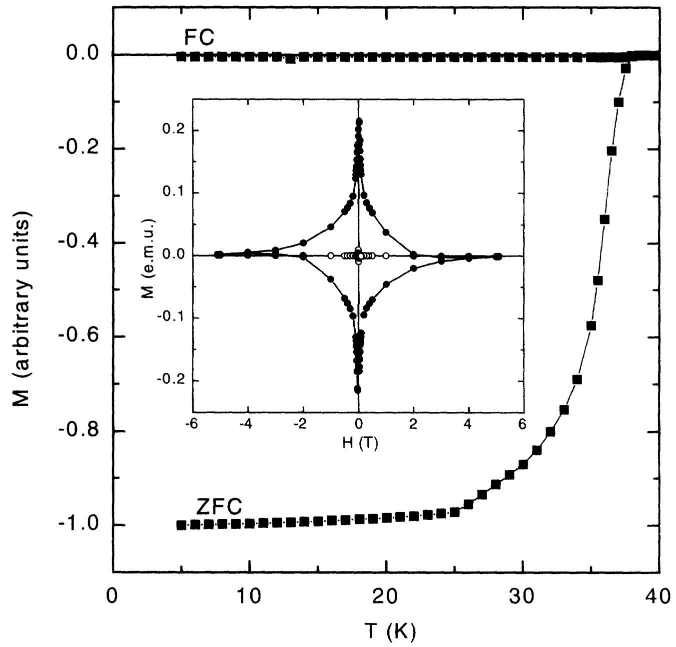

Fig. 1 (left). Resistivity (ρ) versus temperature for a MgB$_2$ thin film grown on an AO substrate by means of using pulsed laser deposition with post-annealing techniques. The inset is a magnified view of the temperature region from 36 to 40 K, for the sake of clarity. A sharp superconducting transition is observed at 39 K. **Fig. 2 (right).** Magnetization versus temperature at $H = 10$ Oe for a MgB$_2$ thin film. The inset shows the M-H hysteresis loop at 5 K (solid circles) and 35 K (open circles). Very high current-carrying capabilities of ~6 × 10^6 A/cm^2 at 5 K and ~3 × 10^5 A/cm^2 at 35 K were observed at zero field.

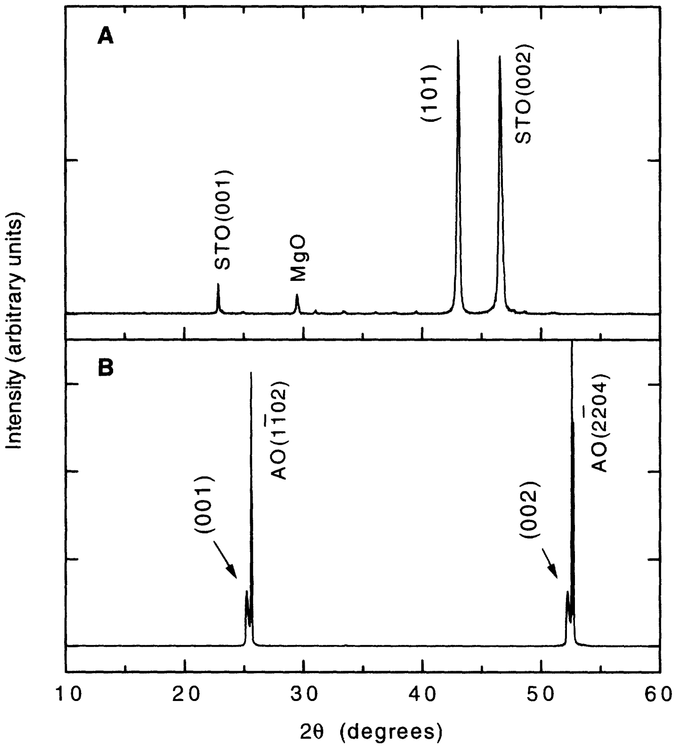

Fig. 3. XRD patterns for MgB$_2$ thin films grown on (**A**) (100) STO and (**B**) $(1\,\bar{1}\,0\,2)$ AO substrates. The (00l) peaks of MgB$_2$ grown on AO indicate c axis–oriented epitaxial thin films, whereas MgB$_2$ deposited on STO shows (101) plane-oriented thin films.

We used a two-step method to fabricate MgB$_2$ thin films. First, we deposited amorphous B thin films; we sintered them at high temperature in Mg vapor, a process very similar to the growth techniques for cuprate Hg-based superconducting thin films (*12*, *13*). We pressed commercial B (99.99% pure) powder into a disk shape with a diameter of 12.7 mm and a height of 5 mm under a pressure of 6 tons. Precursor thin films of B were deposited on Al$_2$O$_3$ (AO) and SrTiO$_3$ (STO) substrates at room temperature by means of pulsed laser deposition. The laser energy density was 20 to 30 J/cm^2 at a laser flux of 600 mJ per pulse and a pulse frequency of 8 Hz. After a precursor thin film had been fabricated, it was put into a Ta tube together with a high-purity Mg metal (99.9% pure) and sealed in an Ar atmosphere. The heat treatment was carried out in an evacuated quartz ampoule to prevent oxidation of the Ta tube. The typical sintering procedure was fast heating to 900°C in 5 min; this temperature was held for 10 to 30 min and then quenched to room temperature. The typical film thickness used in this study was 0.4 μm, which was measured by a scanning electron microscope. This simple technique can be applied to other physical deposition methods, such as sputtering and electron-beam evaporation, and is highly reproducible, so mass production should be possible. The resistivity measurements were carried out using the dc four-probe method. The dc magnetic properties were measured with a Quantum Design MPMS superconducting quantum interference device (SQUID) magnetometer. The structures were analyzed with an x-ray diffractometer (XRD).

The typical temperature dependence of the resistivity of MgB$_2$ grown on AO is shown in Fig. 1. The inset is a magnified view near the T_c region. The resistivity of the film begins to enter the superconducting transition at 39 K and goes to zero resistance at 37.6 K. A very sharp transition, with a width of ~0.7 K from 90 to 10% of the normal state resistivity, is evident in the inset (Fig. 1). This is comparable to most reported values for high-quality bulk samples (*3–6*). The normal-state resistivity at 290 K was $\sim$4.7 $\mu\Omega \cdot$ cm, indicating an intermetallic nature with a relatively high charge carrier density (*2*). This resistivity is smaller than those for polycrystalline MgB_2 wire (*10*) and for bulk samples synthesized under high pressure (*3*, *4*). Most of our films fabricated under the same conditions showed a similar superconducting transition around 39 K.

Figure 2 shows the zero-field–cooled (ZFC) and the field-cooled (FC) dc magnetization (M) curves of a MgB_2 thin film in a 10-Oe field applied parallel to the c axis. The irreversibility temperature detected at 37.5 K coincides with the zero-resistance temperature obtained from measurements of resistivity. The ZFC curve shows a rather broad diamagnetic transition as compared to the resistivity data. To estimate the critical current density (J_c), we measured the M-H (H is magnetic field) loop for the same sample as a function of temperature, as shown in the inset of Fig. 2. At zero field, the J_c calculated with the Bean model was $\sim 6 \times 10^6$ A/cm^2 at 5 K and $\sim 3 \times 10^5$ A/cm^2 at 35 K, values that are 10 times higher than the values obtained for a MgB_2 wire (*10*) by means of transport measurements and slightly smaller than the values for Hg-based superconducting thin films (*12*). It should be noted that we used the sample size rather than the grain size in calculating J_c. In view of the strongly linked nature of the intergrains (*9*) and their excellent electrical and magnetic characteristics as compared to conventional superconductors, these films would be useful in electronic device applications, such as microwave devices and portable SQUID sensors, by using miniature cryocoolers with low power consumption.

Structural analysis was carried out by XRD (Fig. 3). The a- and c-axis lattice constants determined from the (101) and the (00l) peaks are observed to be 0.310 and 0.352, respectively. The XRD patterns indicate that the films deposited on AO (Fig. 3A) are epitaxially aligned with the c axis, whereas the films on STO (Fig. 3B) are well aligned with the (101) direction normal to the substrate planes. These results suggest that we may be able to control the orientation of MgB_2 thin films simply by using different substrates if the optimum growth condition is explored. We also find that the AO substrates are chemically very stable during heat treatment at high temperatures in Mg vapor. With its high thermal conductivity and small dielectric constant, AO is a very promising substrate for use in superconducting device applications, such as microwave devices and portable sensors. For the STO substrates, however, a chemical reaction between the substrate and Mg was observed and appeared as minor impurity phases (Fig. 3A). Considering that STO has a cubic structure with a lattice constant of 0.389 nm and that R-plane AO has a_0 = 0.476 nm and $b_0^* = (c_0^2 + 3a_0^2)^{1/2}$ = 1.538 nm, it is quite striking that MgB_2 thin films grow with preferred orientations on AO and STO substrates even though the lattice-matching relationship between the MgB_2 and the substrates is not well satisfied.

References and Notes

1. J. Nagamatsu *et al.*, *Nature* **410**, 63 (2001).
2. W. N. Kang *et al.*, preprint available at http://xxx.lanl.gov/abs/cond-mat/0102313 (2001).
3. C. U. Jung *et al.*, preprint available at http://xxx.lanl.gov/abs/cond-mat/0102215 (2001).
4. Y. Takano *et al.*, preprint available at http://xxx.lanl.gov/abs/cond-mat/0102167 (2001).
5. D. K. Finnemore *et al.*, *Phys. Rev. Lett.* **86**, 2420 (2001).
6. H. Kotegawa *et al.*, preprint available at http://xxx.lanl.gov/abs/cond-mat/0102334 (2001)
7. G. Karapetrov *et al.*, preprint available at http://xxx.lanl.gov/abs/cond-mat/0102313 (2001).
8. S. L. Bud'ko *et al.*, *Phys. Rev. Lett.* **86**, 1877 (2001).
9. D. C. Labalestier *et al.*, *Nature* **410**, 186 (2001).
10. P. C. Canfield *et al.*, *Phys. Rev. Lett.* **86**, 2423 (2001).
11. A. Gupta, J. Z. Sun, C. C. Tsuei, *Science* **265**, 1075 (1994).
12. L. Krusin-Elbaum, C. C. Tsuei, A. Gupta, *Nature* **373**, 679 (1995).
13. W. N. Kang, R. L. Meng, C. W. Chu, *Appl. Phys. Lett.* **73**, 381 (1998).

14. Supported by the Creative Research Initiatives of the Korean Ministry of Science and Technology.

19 March 2001; accepted 2 April 2001
Published online 12 April 2001;
10.1126/science.1060822
Include this information when citing this paper.

Hydrated Salt Minerals on Ganymede's Surface: Evidence of an Ocean Below

Thomas B. McCord,* Gary B. Hansen, Charles A. Hibbitts

Reflectance spectra from Galileo's near-infrared mapping spectrometer (NIMS) suggests that the surface of Ganymede, the largest satellite of Jupiter, contains hydrated materials. These materials are interpreted to be similar to those found on Europa, that is, mostly frozen magnesium sulfate brines that are derived from a subsurface briny layer of fluid.

Ganymede is the third outward and the largest of Jupiter's four major satellites, named the Galilean satellites after their discoverer. These satellites range in size from slightly smaller than the Moon to larger than Mercury and are large enough to have undergone at least some internal thermal evolution and differentiation (*1*). There are three major sources of internal heat to support thermal evolution: (i) decay of radioactive isotopes; (ii) tidal dissipation, which is more effective on satellites closer to Jupiter; and (iii) differentiation, resulting from the first two processes. These processes operate on different time scales. Thus, the thermal evolution of these satellites should be complex and different for each satellite. Evidence of these processes should exist in the composition of the surface material. Because of their distance from the Sun, at the boundary where water ice is stable, these satellites probably formed from material rich in H_2O, such as found in primative meteorites (*2*), and including water ice grains (*3*). Io, the closest Galilean satellite to Jupiter, is the most volcanically active body in the solar system and is thermally processed due to tidal heating such that most or all of the water has been lost. Early ground-based spectroscopic observations (*4*) provided evidence of water ice as a major constituent of the surfaces of the outer three satellites (Europa, Ganymede, and Callisto). Water ice on the surface is probably the result of thermal processing of water and water-bearing material originally forming the satellites, leading to differentiation and migration of water to the surface layers and production of hydrated minerals as water circulates through and leaches ions from the satellite materials (*5–8*). Recently, the NIMS provided evidence of materials other than water ice on the icy satellites (*9*). These include non–water ice but H_2O-bearing material on Europa. The material is preferentially located in the lineaments and chaos terrain (recently disrupted areas) and was interpreted to be mostly hydrated salt minerals, mostly $MgSO_4$ and possibly Na_2SO_4, derived from a briny ocean below the ice crust (*10–12*). H_2SO_4 hydrate also has been suggested as a constituent due to radiolysis of sulfur and ice at the surface (*13*). Some H_2SO_4 hydrate could be present as a result of radiation processing of the minority Na_2SO_4 hydrate mixed with the majority $MgSO_4$ hydrate (*12*, *14*). Hydrated salt minerals on and in the more processed icy satellites are predicted by models of the thermal evolution of the Galilean satellites and studies of carbonaceous chondrite meteorites (*5–8*).

Evidence of hydrated minerals on the surface of the Galilean satellites comes from infrared reflectance spectra. Water molecules

---

Hawaii Institute of Geophysics and Planetology, University of Hawaii, Honolulu, Hawaii.

*To whom correspondence should be addressed. E-mail: tom@higp.hawaii.edu